Energy Conversion and Management 314 (2024) 118633

Contents lists available at ScienceDirect

Energy Conversion and Management

journal homepage: www.elsevier.com/locate/enconman

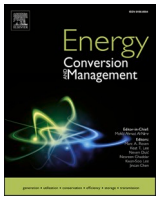

Research Paper

Analysis of indirect power cycles for a novel methanol-to-methane TCES-CSP system

D.A Rodriguez-Pastor [a,*], I. Marqués-Valderrama [a], V.M Soltero [b], R. Chacartegui [a,c]

[a] University of Seville, Escuela Técnica Superior de Ingenieros, Camino de los Descubrimientos s/n, 41092 Seville, Spain
[b] University of Seville, Escuela Politécnica Superior, 41011 Seville, Spain
[c] University of Seville, Laboratory of Engineering for Energy and Environmental Sustainability, Seville 41092, Spain

ARTICLE INFO

Keywords:
Thermochemical energy storage
Methanol
Methane
CSP
Power cycles

ABSTRACT

The security of the supply of clean energy resources and the production of renewable fuels for industry are some of the strategies to combat climate change. In this sense, the massive implementation of green fuels that is foreseen forces the industrial park to operate on hydrogen and/or ammonia, methanol and others, with a cost overrun for stakeholders. This work proposes an alternative through a methanol-to-methane conversion system from the intermediate step to synthesis gas. Methanol decomposition is a process that can be produced with solar energy (CSP) at moderate temperatures (<350 °C) and at low cost, whereas methanation is a well-known and industrially mature process that occurs at temperatures < 625 °C. The integration of both processes is employed as a method of solar storage, namely through high-pressure syngas and its discharge for power production in conventional cycles. Recuperative ORC configurations, Rankine steam, and a sCO2 Brayton cycle were integrated; all of them of techno-economic interest, offering round-trip efficiencies higher than 50 % and levelized costs (LCOE) lower than EUR 55/MWh, considering a high-energy methane stream at the outlet. This offers a system that proposes a solution for the massive deployment of methanol as a green hydrogen carrier molecule, where it is capable of cleanly and efficiently storing thermochemical energy and producing high-purity methane at the output, usable in other power cycles, or as an industrial feedstock.

1. Introduction

Security in the supply of clean, sustainable, and efficient energy is one of the fundamental pillars of society in the current decade of the 2020 s [1]. Geopolitical conflicts have forced institutions to develop alternative energy production strategies to avoid dependence on foreign resources [2,3]. The European Union has launched the REPowerEU plan in response to disruptions in the energy market caused by the Russian invasion of Ukraine in 2022, which sets a target of 10 million tons of renewable fuels of non-biological origin in 2030 (14 % of the total EU electricity consumption) and is reflected in the Commission's proposal to set 45 % as the EU target for renewable energy by 2030 [4]. In this sense, the production of non-biological renewable fuels, together with the massive deployment of renewable energy, implies scenarios that are expected to provide a solution to the goals set by COP21 [5]. Energy storage is a key element in the transition to a fully renewable and sustainable generation system [6], where energy production and demand are decoupled [7].

Although a massive deployment of hydrogen-derived renewable fuels is expected, few studies have considered the intermediate reactions of *green molecules* (green hydrogen-based fuels) decomposition/synthesis for energy storage. Similarly, there is no evidence of large projects related to its direct conversion to other chemicals from concentrated solar power, where the integration of the chemical process allows solar energy storage. Concentrating solar power (CSP) technology for energy storage is of special interest owing to its dispatch potential and scalability, especially for sensible heat [8], with costs of an order of magnitude lower than those of electrochemical batteries (€300-400/kWh) [9]. In recent years, different concepts of storage integration with CSP have been proposed, using i) molten salts for sensible heat storage (SHS), with great maturity in the industry [10]; ii) latent heat storage (LHS) from the phase change of materials (PCM), as reviewed in [11]; and iii) thermochemical energy storage (TCES) from the integration of reversible charge and discharge reactions and storage in chemical bonds [12]. Similar concepts have been presented for chemical conversion systems for the storage and subsequent use of chemical products

* Corresponding author.
E-mail address: drodriguez4@us.es (D.A Rodriguez-Pastor).

https://doi.org/10.1016/j.enconman.2024.118633
Received 9 March 2024; Received in revised form 28 May 2024; Accepted 29 May 2024
Available online 8 June 2024

obtained in the discharge or exothermic phase, proposing cogeneration [13], trigeneration [14] or polygeneration systems [15].

Chemical heat storage (CHS) can be classified into two categories depending on the reaction mechanism: through chemical reaction pairs of solid–gas, liquid–gas and gas–gas (without sorption) and through chemical sorption heat storage. TCES systems based on the CHS principle require an external source of energy in the charge phase, where the reactant decomposes into an endothermic reaction. From the subsequent compression of the reaction product, it can be stored and released in the discharge phase, where it is synthesised through an exothermic reaction that releases heat, which is usable in applications such as district heat networks [16] or in a power block [17], depending on the temperature limit imposed on the reaction. Several types of TCES are currently being investigated on a pilot scale, including those based on hydroxides [18], carbonates [19], ammonia [20], and methanol [21]. Decomposition reactions that require a lower reaction temperature will be of greater interest because they will allow for lower-cost thermal integration from solar energy, and the high heat of reaction synthesis reactions that are highly exothermic will allow greater heat utilisation and a better round-trip efficiency of the system (RTE). In addition to the use of stored chemical heat, the heat stored in the by-products of reactions incurs a higher energy density compared to commercial TES molten salt systems (~0.5 GJ/m^3) [22]. As energy is stored in chemical form, products from the decomposition phase can be stored at ambient temperature, reducing thermal losses and unlocking long-term storage.

Several studies have explored different configurations of solar TCES with power blocks, such as [23] or [24] in calcium looping, achieving a global energy efficiency of 45 % with a closed Brayton cycle with carbon dioxide. CSP-TCES alternatives for redox, hydroxide, and carbonate reactions were studied in [25] determining that the former has the highest solar-to-electric efficiency and the latter has the lowest LCOE. For gas-to-gas systems, the integration of ammonia thermochemical storage of ammonia (~650 °C) with a 10 MWe steam turbine was analysed [26], as well as for a supercritical steam cycle, resulting in complex and expensive systems given the high reaction temperatures [27]. A mid-temperature solar system converting methanol to syngas and 20 kWe in an ICE was studied in [28], reaching a solar-to-electric efficiency of 18.29 %. Rankine cycles are the most usual integration in the solid-to-gas and gas-to-gas TCES-CSP due to better thermal performance in the medium temperature range and the maturity of the technology. Unlike previous TCE approaches, the integration proposed in this work allows the use of the product at the outlet during the discharge phase.

Similarly, new techniques to obtain synthetic natural gas (SNG) from energy carriers with high energy density are necessary, as they enable the sustainability of energy and industrial systems without having to modify the existing industrial park. Currently, switching the thermal generation industry fleet to hydrogen involves a cost overrun of 60 % [29]. Other green molecules, such as methanol or ammonia, have half the heating value of natural gas (143 MJ/kg H_2 > 50 MJ/kg CH_4 > 22.5 MJ/kg NH_3 > 19.9 MJ/kg CH_3OH), which incurs lower thermal efficiencies [30,31]. The present work provides an answer to the integration of renewable fuels into industrial processes, also providing an alternative energy storage strategy, since it identifies the advantage that they have a higher volumetric energy density than natural gas at ambient pressure (15.6 MJ/L CH_3OH > 12.7 MJ/L NH_3 > 0.0364 MJ/L NG > 0.0107 MJ/L H_2) [30,32], incurring considerably reduced transport costs [33]. Therefore, green fuels can be synthesised cleanly in places far from the consumption point, allowing the flexible generation of thermal, chemical, or power energy. Furthermore, some studies have estimated that green fuels, such as renewable methanol, could reach fossil fuel prices by 2030 [34].

This article studies power block integrations into a novel concept for thermochemical energy storage. It is based on a novel two-stage concept, the conversion of methanol to syngas and syngas to methane in an open cycle, an approach developed in the patent of Chacartegui et al. [35]. Closed-loop configurations were studied by Rodriguez-Pastor et al. [21,36] with RTE efficiencies of 44 % and levelized cost of electricity (LCOE) below €265/MWh were obtained. Power block-TCES integration is studied with high-temperature organic fluids, steam and supercritical CO_2. The presented approach presents a competitive levelized cost of energy as it considers the joint production of electricity, heat and methane (as feedstock). It is shown as a feasible solution based on processes well-known processes in the industry and reactions that can occur with low-cost catalysts. Green methanol production is expected to grow considerably in the coming years, and the proposed system does not compromise the existing industrial park, as it converts it to green natural gas without additional cost overruns for stakeholders.

2. System description

2.1. Methanol-to-methane TCES

The proposed thermochemical storage system makes use of concentrating solar energy for the thermal decomposition of methanol (Fig. 1). This reversible reaction occurs at a moderate temperature of 315 °C and pressure of up to 25 bar. Under these conditions, the integration of solar thermal systems is possible, either by a central receiver or parabolic trough, as employed in this work. In the open cycle mode, methanol is decomposed into synthesis gas (phase 1), which is compressed and stored at ambient temperature. Subsequently, in phase 2, the synthesis gas (CO/H_2) is synthesised by the methanation process, recovering exothermic energy from a network of exchangers in a cycle or power block. The products resulting from the separation can be easily separated in a flash vessel by dew point difference to obtain high-purity methane that can be used in a power cycle as a gas turbine Brayton or as a feedstock for the chemical industry.

This system has several advantages. The methanol-to-methane conversion system allows direct use of existing conventional equipment and processes. Methanol management is easier than that of other green hydrogen carriers. It can be stored in liquid form at ambient temperature, reducing storage volumes. Methanol is a mature chemical widely used in the industry, and as fuel, it is a candidate for future green fuel in marine propulsion. Methanol can be transported by truck or ship to the facility's destination or produced on-site from a green hydrogen facility.

From its decomposition (**Eq. (1)**), a synthesis gas is obtained that can be used directly in power cycles, such as gas turbines [37] and ICEs [28]. In the proposed configuration, this mixture of carbon monoxide and hydrogen is compressed to high pressure and cooled to ambient temperature by the proper thermal integration of a simple heat exchanger network.

$$CH_3OH \rightleftarrows CO + 2H_2 \quad \Delta H_{298K} = 90.7 kJ/mol \tag{1}$$

Fig. 2 shows the process flow diagram of the charge phase of the storage process, in which methanol is pumped up to 10 bar (*stream 2*),

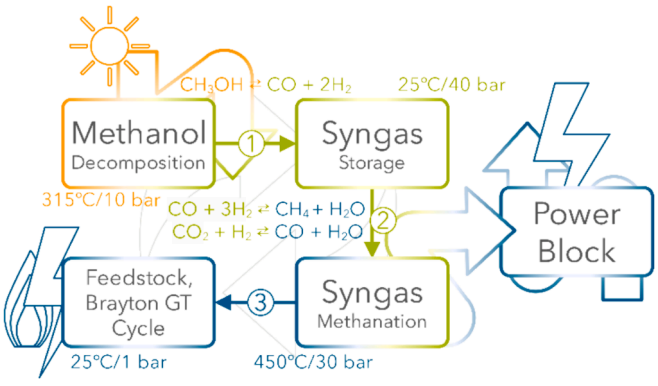

Fig. 1. Schematic route of methanol-to-methane conversion, indicating the processes carried out and operating conditions in each case.

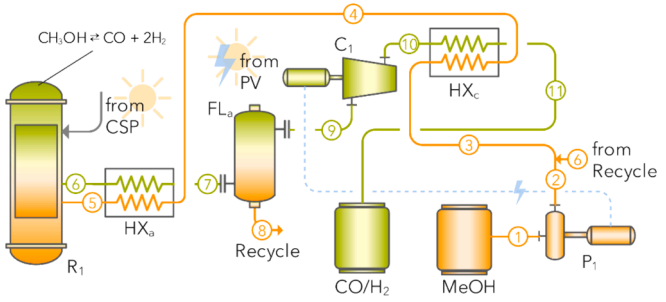

Fig. 2. Conceptual scheme of methanol-to-synthesis gas decomposition process (charge phase of the proposed TCES). Green and orange streams represent synthesis gas and methanol (MeOH) streams, respectively. The blue dashed lines represent the electricity consumption provided by the solar photovoltaic energy. The grey line refers to the passage of energy coming from a CSP parabolic through collector plant. (For interpretation of the references to colour in this figure legend, the reader is referred to the web version of this article.)

passing through a network of exchangers (HX_b) that exchange heat with the syngas at high temperature and pressure from the decomposition of methanol (*stream 10*). The electricity consumption for the pressure-boosting equipment is provided by a photovoltaic plant (*PV*) that can be located close to the site, given its limited consumption (<5 MW) and low land requirements. After passing through a preheater (HX_a), methanol enters under gaseous conditions into fixed-bed reactor R_1 (solar receiver) producing synthesis gas (*stream 6*), in which there may be unreacted methanol that will be separated by the flash separator (FL_a) and returned to the cycle (*stream 8*) to obtain full conversion in the reaction. The syngas obtained (*stream 11*) is stored and discharged when the power or heat demand is required.

A process with great maturity in the industry, which is a novelty reflected in the patent published by the authors [35], involves the methanation of the generated syngas. This highly exothermic process (**Eq. (2)** is favoured by low temperatures according to LeChatelier's principle, which can occur at temperatures of up to 600–700 °C, such as in the commercial TREMP™ reactor [38]. These temperatures can be lowered depending on the type of catalyst and reactor, making them more suitable for the integration of a power block, as discussed in the following sections.

$$CO + 3H_2 \rightleftarrows CH_4 + H_2O \Delta H_{298K} = -206.1 kJ/mol \quad (2)$$

When the syngas in the charging phase is compressed to high pressure, its discharge will be able to recover energy (HX_d, HX_e) through an expansion process (Expanders Exp_1 and Exp_2, in Fig. 3). Furthermore, they also help to lower the temperature of the by-products formed in the methanation reactor (R_2) until the ambient temperature of the methane and water formed by the reaction is reached (*streams 23 and 24*). Thus, both species can be separated in a flash separator (FL_b) to obtain high-purity methane that can be used in a gas turbine cycle, in cogeneration engines, or in the chemical industry. This fact implies that if, economically, methane increases its price, as predicted by different studies [39–41] green hydrogen price decreases [30] (and therefore, the price decreases for e-methanol [42]), and this system could pose alternative business strategies for the use of green fuels in large industries, given its scalability and dispatchability.

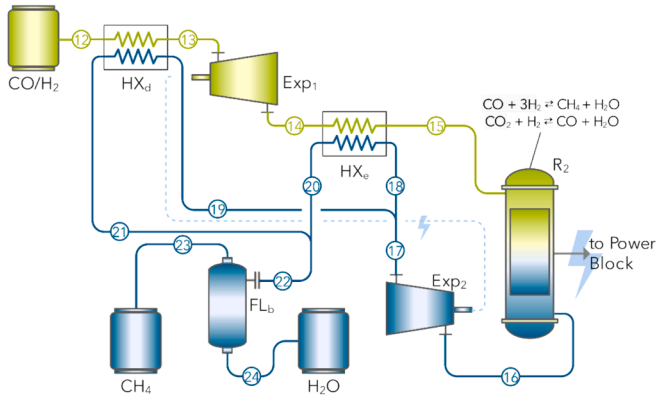

Fig. 3. Conceptual scheme of the discharge phase in the proposed TCES system, where syngas is converted to methane. The green lines indicate syngas, and the blue lines represent a mixture of the reaction products, methane (CH_4) and water (H_2O). The dashed blue lines represent the flows of electrical energy generated by the expander generators. (For interpretation of the references to colour in this figure legend, the reader is referred to the web version of this article.)

2.2. Power cycle integration

Currently, the most productive CSP plants are based on superheated steam cycles with a maximum temperature of approximately 560 °C to allow integration with molten salt storage [23]. This current CSP innovation presents a global efficiency of approximately 38 %, with a yearly solar-to-electrical efficiency lower than 20 % [43]. Few studies have considered the integration of power blocks into gas-to-gas TCES systems. Chen et al. demonstrated the feasibility of heating supercritical steam up to 650 °C using ammonia synthesis, which was validated in a 15 kWt pilot-scale prototype. Ammonia-based storage has challenges ranging from gas safety to economic evaluation [44]. Other configurations based on SO_3 and its dissociation to SO_2 (based on sulphur) pose greater complexities because they have an additional step in the reaction [45] in addition to being highly corrosive. Those based on cyclohexane dehydrogenation pose problems of reversibility and toxicity, making them complex for CSP implementation. Peng et al. [46] developed the first techno-economic study of a methane-reforming TCES system coupled with a power block. By harnessing the exothermic heat in a turbine, the system reached solar-to-electric efficiencies of 17.1 % and an LCOE of 9.6 cents/kWh.

There are two possible integrations of the power block: the indirect one from the thermal exploitation of the exothermic reaction utilising independent streams heated from a network of exchangers and from a direct simple or combined gas turbine cycle, making use of methane at the outlet of the discharge phase as fuel in the combustion chamber, as analysed by the authors in [36]. This work focuses on the analysis of simple and recuperative organic Rankine cycles, for four fluids that can operate at temperatures ~ 450 °C without suffering thermal degradation, as well as a reheated steam Rankine cycle and a supercritical CO_2 Brayton cycle (Fig. 4). All fluids are known in the industry, and simulation models can be developed using zero-dimensional (lumped-

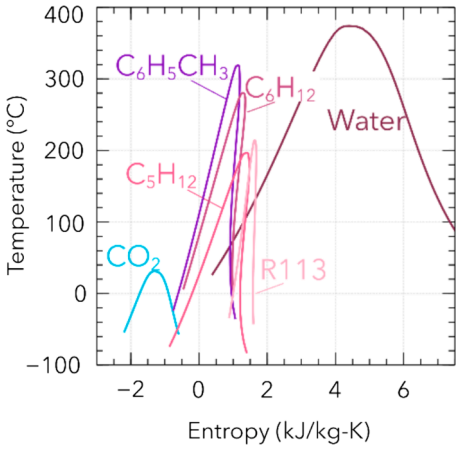

Fig. 4. T-s (temperature-entropy) diagram of the studied working fluids for the power block in this work (CSP MeOH-CH_4 TCES).

volume) approaches [47]. The main challenge of the proposed system lies in the integration of the heat exchanger into a multistage methanation reactor. The indirect integration of the power cycles allows the independence of the reaction conditions from the power block without affecting the turbine conditions [17].

2.2.1. Organic Rankine cycle

High-temperature organic fluids have been considered (Table 1) for evaporation from the heat of the methanation reaction [48]. The expansion occurs when the maximum possible temperature is reached, which is the reaction temperature. The configurations studied were the simple ORC cycle and ORC recuperative cycle, where the positive slope of the saturated steam curve is of interest for the former.

The evaporating pressure is given by the critical pressure of the working fluid and is higher (considering an overheating of 10 K) in the recuperative case. Both configurations operated at the same condensing pressure set by the condensing tower. Fig. 5**A** shows the organic Rankine cycle in a simple cycle, where the heat generated in the reaction is recovered from the products of the reaction and leads to the evaporation of the fluid (*stream 2*). For the recuperative cycle (Fig. 5**B**), the input conditions for the evaporator (*Evap*) were given by the output of the recuperator (*Rec.*), where the pump output (P_{ORC}) is preheated to the liquid state (*Stream 2*). According to Schmidt et al. [49], the recuperative option for toluene as the working fluid will be of greater interest in terms of the thermal efficiency of the cycle, demonstrating a 41.9 % efficiency result. The ORC-based power block has lower complexity in terms of heat integration, especially for powers not exceeding 10 MW, due to its modularity. By operating at lower evaporation pressures than other cycles, i.e. steam Rankine, the components have lower design requirements and present better durability in materials, making them more compatible with solar energy storage systems. In addition, it can be adapted to different temperature levels and power output requirements. One of the challenges is the high specific cost and costs associated with operation and maintenance [50].

2.2.2. Steam Rankine cycle

Steam power plants are mature in the industry and are of great interest for integration into energy storage systems, given their efficient electrical energy production. Studies related to the evaluation of these cycles offer efficiency values of 42 %, which can be higher for higher reaction temperatures, and therefore, higher inlet temperatures for the steam turbine. The steam pressures are completely independent of the reaction pressures of the discharge phase of the TCES system, which makes it of special interest for indirect integration. The condensation pressure is determined by the type of cooling used; in this case, a cooling tower was employed.

Fig. 6 shows the conceptual process flow diagram of the Rankine steam cycle system with reheat (*Reheat*), in which there are two steam extractions from the high-pressure turbine (T_{HP}) and three from the low-pressure turbine (T_{LP}). Thermal recovery from the methanation reactor is split into two energy streams to the heat exchanger HX_e and the Reheater (*Reheat*). The steam reheat configuration offers a higher efficiency without compromising the initial power block investment costs.

2.2.3. Supercritical CO_2 brayton cycle

Carbon dioxide has a reduced critical temperature and thermal properties of interest. This work considers a supercritical CO_2 cycle, which takes advantage of the maximum inlet temperature to the power block, imposed by the reaction temperature. According to previous work regarding the optimisation of the performance of the cycle [51], the high pressure was set at 222 bar and the low pressure at 148 bar, reaching cycle thermal efficiencies of 50 %. This type of cycle offers higher efficiency than the rest of the configurations studied, which makes it of interest for power applications that do not require very high temperatures. By using CO_2 as the working fluid, it can take advantage of industrial emission effluents, or it can be directly integrated with solid-to-gas TCES systems that imply carbon capture and storage [52]. The versatility of CO_2 in various fields gives it different opportunities for integration to combat climate change, as demonstrated in the work of our research group [53]. Fig. 7 shows the conceptual diagram of the sCO_2 cycle, in which integration with the methanation reactor (R_2) is performed from the heat exchanger (HX_a), starting from *stream 4*. A recuperator (*Rec*) is used to preheat the input to the HX_a exchanger as it passes through the T_{CO2} turbine after being compressed in the C_{CO2} compressor stage.

Table 1
Critical temperatures (K) and pressures (bar) for organic working fluids considered in ORC power block.

Working fluid	T_{crit} (K)	P_{crit} (bar)
Cyclohexane	553.6	45.1
n-Pentane	470	33.3
Toluene	407.8	41.08
R113	487.2	33.9

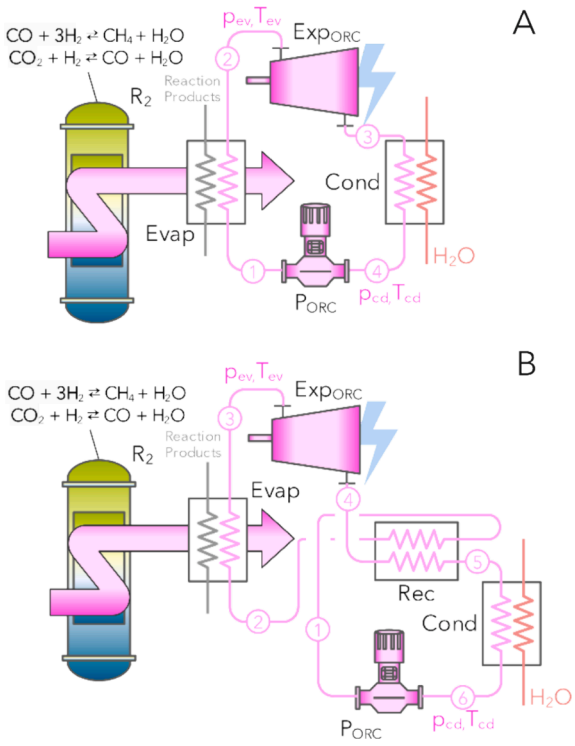

Fig. 5. Process flow diagrams for organic Rankine cycle configurations. A. Simple ORC cycle B. Recuperative ORC cycle. Pink streams indicate organic fluid flow; red streams indicate water flow; Evap (ev): Evaporator, Cond (cd): Condenser, Exp_{ORC}: Expander, P_{ORC}: Pump, R_2: Methanation reactor. (For interpretation of the references to colour in this figure legend, the reader is referred to the web version of this article.)

3. Modelling

3.1. Charge Phase: Direct (thermal) decomposition of methanol (CH_3OH)

The decomposition of methanol (MeOH) into CO/H_2 (syngas) can occur via direct (thermal) decomposition, steam reforming, partial oxidation, and autothermal reforming, as reviewed in [21]. It is a promising reaction for CSP-TCES as it occurs at temperatures below 350 °C, and the required catalysts are well-known in the industry. Direct (thermal) decomposition of methanol from solar energy is a complex process involving the dissociation of methanol by filling the reactor bed (solar receiver) commonly with a porous $Cu/ZnO/Al_2O_3$ catalyst.

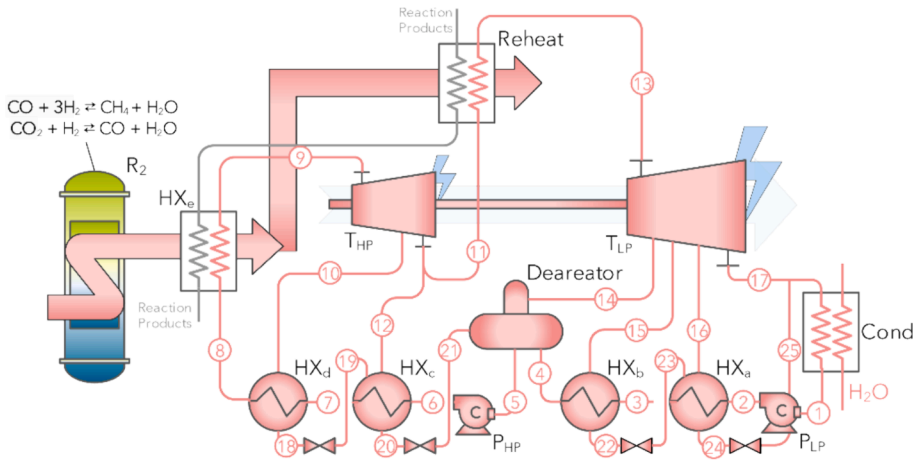

Fig. 6. Conceptual process flow diagram of the power block based on superheated steam Rankine cycle. Red lines indicate water or steam. P: Pump, T: Turbine, Cond: Condenser, HX: Heat Exchanger. R_2: Methanation Reactor. (For interpretation of the references to colour in this figure legend, the reader is referred to the web version of this article.)

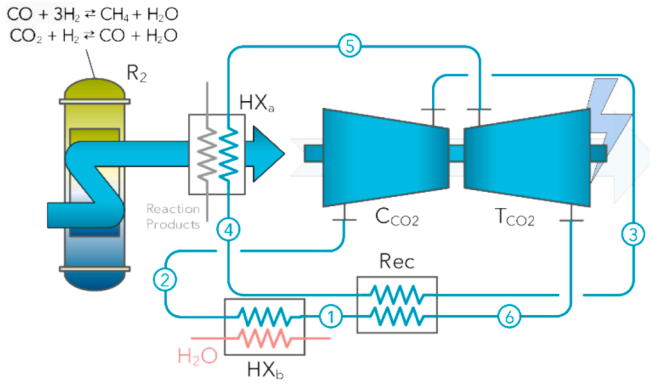

Fig. 7. Conceptual process flow diagram of the sCO2-based power block. Cyan lines indicate CO2 flow and red lines indicate water flow. C: Compressor, HX: Heat Exchanger, Rec: Recuperator, R2: Methanation Reactor, T: Turbine. (For interpretation of the references to colour in this figure legend, the reader is referred to the web version of this article.)

Complete conversion can be obtained at ambient pressure and temperatures of 315 °C.

The model was simulated using the commercial software ASPEN HYSYS from a plug flow reactor (PFR) and the Peng Robinson thermodynamic method. The analysis of the kinetic constants of the model according to Hou et al. [54], as well as the properties of the used catalyst, are detailed in Appendix A. Operating conditions of the charge phase of the TCES system are listed in Table 2. For the system simulation, a quasi-dynamic evolution was considered, in which the charge hours were defined by the solar resources available for the site under study. The concept of peak sunhours (at the case site 1 kWh/m^2) at which the system operates at the design point was considered. Transient models were not considered because the storage was sized to cover at least three days of discharge operation, providing sufficient inertia for a continuous operation.

Table 2
Thermodynamic operating considerations for the charge phase of the plant proposed in this work.

Variable	Value
Inlet CH_3OH molar flow	100 mol/s
CH_3OH storage temperature/pressure	64.67 °C/1 bar
Isentropic efficiency of liquid methanol pump	65 %
Isentropic efficiency of compressors	89 %
Heat Exchangers approach temperature	20 K
Endothermic reaction temperature/pressure	315 °C/10 bar
Syngas CO/H_2 storage pressure	40 bar

The studied power plant site was Seville, Andalusia, Spain (Lat./Long.: 37.383°/-5.973°), considered due to a significant annual solar resource (Fig. 8) that allows obtaining 2220 full load annual operation hours [55], It allows an average charge-phase operation of 6 h, offering 18 h of stored discharge in the form of synthesis gas after the operation of three consecutive cycles. The PV system has been defined based on the methanol pumping power and compression syngas power requirements of the charge phase, dependent on the cycle conditions; a typical ground coverage ratio value of 0.48 has been considered to determine the required land use [56]. The modelling of the photovoltaic installation has been carried out in the PVSyst software [57], for the PV module of Jinko brand of 575 Wp of maximum power (model JKM575M-7RL4-V), grouped in strings with trackers on a horizontal axis, resulting in 2780 total PV modules and 3.33 ha of photovoltaic field required area. The commercial inverter used in the installation is the KSTAR GSM1500, with 1,500 kW, resulting in ~ 2,490 MWh/year of electricity production at the study site (PR = 85.3 %).

3.2. Discharge phase: CO methanation

One of the novelties of this system is the synthesis of syngas that is

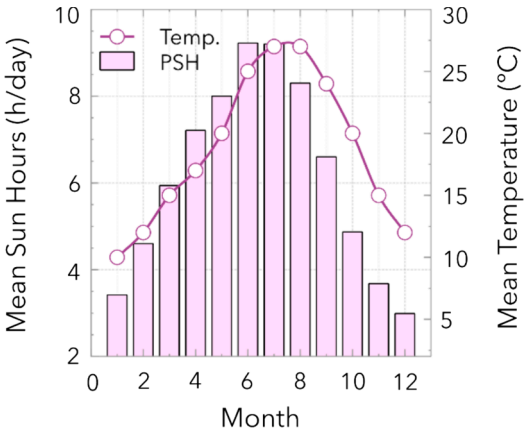

Fig. 8. Mean monthly solar hours (left y-axis) and mean monthly dry temperatures (°C) (right y-axis) for the site selected in this study.
Source: Technical Building Code in Spain and [55]

produced during the decomposition of methanol into methane. CO methanation is a well-known industrial process with a high reaction enthalpy that allows thermal use employing power cycles, as presented in this work. It is thermodynamically feasible and spontaneous at temperatures < 625 °C [58]. Carbon monoxide methanation can be grouped into a combination of three reactions consisting of CO, CO_2, H_2O, CH_4 and H_2, being the main reactions, the methanation of CO and CO_2 (**Eqs. (3), (4)**), coupled with the water gas shift reaction (**Eq. (5)**):

$$CO + 3H_2 \rightleftarrows CH_4 + H_2O \qquad \Delta H_{298K} = -206.1 kJ/mol \tag{3}$$

$$CO_2 + 4H_2 \rightleftarrows CH_4 + 2H_2O \qquad \Delta H_{298K} = -165 kJ/mol \tag{4}$$

$$CO + H_2O \rightleftarrows CO_2 + H_2 \qquad \Delta H_{298K} = -41.2 kJ/mol \tag{5}$$

The methanation discharge phase was evaluated considering the number of hours for which the syngas storage was designed, as discussed in the previous subsection. This number of discharge hours was set to 6 h, considering the meteorological characteristics of the studied site. The discharge hours could vary depending on the demand required and the available level of syngas in storage, which allows the system to be highly flexible and fast-reacting. The thermodynamic assumptions considered for the methanation phase of the TCES system are listed in Table 3.

3.3. Integration of the power block

For this power cycle modelling section, the Aspen HYSYS kinetic model was integrated with the commercial software Engineering Equation Solver (EES) to implement the power cycle. For the thermodynamic and economic evaluation of the system, the solar-to-electric efficiency η_{sol}^{ele} is defined, which quantifies the energy obtained by the power block from the solar energy (CSP and PV) input to the system in the charge phase, according to the hours of sun per year (**Eq. (6)**.

$$\eta_{sol}^{ele} = \frac{(\dot{W}_{PB} + \dot{W}_{exp})h_{dis}}{(\dot{W}_{PV} + \dot{Q}_{deco})h_{ch}} \tag{6}$$

On the other hand, the overall round-trip efficiency *RTE* evaluates the conversion of input solar energy and methanol energy in the charge phase to methane and power production in the corresponding power block (**Eq. (7)**.

$$RTE = \frac{\left(\dot{W}_{PB} + \dot{W}_{exp}\right)h_{dis} - \dot{W}_{PV}h_{ch}}{(\dot{m}_{CH_3OH}HHV_{CH_3OH} + \dot{Q}_{deco})h_{ch}} \tag{7}$$

3.4. Economics

For the economic evaluation, correlations based on the development of the components and their technology were used, taking references to the approximation of the TCES and renewable energy facilities model listed in Appendix C. The economic evaluation of the power cycles will be given by the characteristics of the cycle equipment, where the CEPCI index [59] adjusted to inflation in 2020 by an annual update factor have been used $\left(I/I_{ref} = 2171.6/800 = 2.71\right)$. This study did not consider scaling factors for power plants with capacities greater than 10 MW. The investment cost estimation equation is given by **Eq. (8)**: [67]

Table 3
Thermodynamic operating considerations for the discharge phase of the plant proposed in this work.

Variable	Value
Inlet syngas molar flow	99.16 CO/198 H_2 mol/s (297 mol/s)
Isentropic efficiency of expanders	92 %
Heat Exchangers approach temperature	20 K
Exothermic reaction temperature/pressure	450 °C/30 bar
Discharge pressure	1 bar

$$C = C_{ref} \cdot \left(\frac{S}{S_{ref}}\right)^m \left(\frac{I}{I_{ref}}\right) \tag{8}$$

C being the cost of the equipment, C_{ref} the reference cost (tabulated in [59]), S the evaluation characteristic magnitude, S_{ref} the reference value of the reference magnitude for the equipment, I the current inflation rate and I_{ref} the base inflation rate for which the reference data is obtained, adjusted by the Marshall & Swift index. Depending on the power cycle, constant values for the investment estimation are detailed in Appendix C. Operating and maintenance costs are estimated at 5 % of CAPEX in each case, considering a renewable methanol cost of €450/ton MeOH [60]. For a useful life (n) of the installation of 25 years and a discount rate (r) of 4.5 %, the Levelized Cost of Energy (LCOE) is employed, expressed in **Eq. (16)**:

$$LCOE = \frac{CAPEX + \sum_{k=1}^{n} \frac{OPEX_k}{(1+r)^k}}{\sum_{k=1}^{n} \frac{\left(E_{PB}^i + E_{exp}^i + E_{CH_4}^i\right)}{(1+r)^k}} \tag{16}$$

CAPEX being the initial investment cost of the plant (TCES and Power Block), $OPEX_i$ is the annual operation and maintenance cost, E_{PB}^i/E_{exp}^i the annual (year i) energy produced in the Power Block/Expanders (discharge phase) in MWh/year. To this energy value is added the energy content of the produced methane, calculated as $E_{CH_4}^i = m_{CH_4}HHV_{CH_4}$ (MWh/year).

4. Results and discussion

For an input thermal solar power in the charge phase of approximately 13 MWt and ~ 1.5 MWe of required electric energy from PV for the compression stage, the results of the integrated methanol-to-methane TCES system are shown in Table 4, after techno-economic optimisation of the processes carried out in which the RTE has been maximised for the minimum LCOE, based on the conjugate variable method in EES software. From the obtained results for the design reaction conditions, in the charging phase, almost all of the methanol reacts according to the experimental data of the employed reactor (0.386 mol s^{-1} CH_3OH reacted/0.39 mol s^{-1} feed for 1000 W m^{-1} [61]) slightly improving the conversion value due to the recycling of unreacted methanol (~99.3 %), while in the methanation kinetic model, a relative error of 13.2 % in the methane yield was obtained compared to the industrial data, comparable to the 12 % relative error associated with the results of the model presented by Er-rbib et al. [62].

The best results are obtained for the supercritical CO_2 cycle, followed by the reheated steam cycle and the recuperative ORC with toluene. For specific cost investments of approximately 2,400 EUR/kW CSP, we propose a system that competes in LCOE with solar PV (~30 EUR/MWh, [63]), given the simultaneous production of electrical power in the power block and expanders and the production of a high-calorific-value methane stream (50 MJ/kg). According to Escamilla et al., the obtained RTE values compete with Power-to-Power storage systems (40–42 %). [64], in addition to compressed hydrogen systems (47 %) at a high storage pressure of 350 bar [65]. One of the disadvantages of the system lies in the low solar-to-electric efficiency (<10 %) since a high methanation pressure is imposed for better conversion to methane, incurring lower electrical power recoveries in the expanders. Considering the thermal efficiency of the power block, lower solar-to-electric efficiencies are incurred despite the high methanation reaction enthalpy. This could be improved by a direct power cycle integration, but the TCES system would lose flexibility under operating conditions, as discussed above.

Fig. 9 shows a summary of the performance of the power cycles studied. In this work, simple ORC cycles have been discarded since they offer a significantly lower thermal efficiency than the rest of the configurations (<25 %). In this sense, the thermal efficiency values are

Table 4
Techno-economic results for integrated power cycles with the proposed TCES.

Power Cycle	RTE (%)	Solar-to-electric efficiency (%)	Power Block (PB) thermal efficiency (%)	Power Block (PB) power output (kW)	Installation CAPEX (EUR)	LCOE (EUR/MWh)
Recuperative ORC						
R113	54.10 %	6.37 %	23.86 %	2707	31,340,000	40.87
n-Pentane	54.45 %	6.70 %	26.22 %	2974	31,425,478	40.73
Cyclohexane	55.84 %	8.06 %	35.73 %	4054	31,686,514	40.09
Toluene	55.92 %	8.14 %	36.28 %	4117	31,639,394	39.97
Steam Rankine	56.44 %	8.66 %	39.87 %	4524	30,647,916	38.37
sCO_2 Brayton	57.85 %	10.04 %	49.54 %	5621	30,959,267	37.85

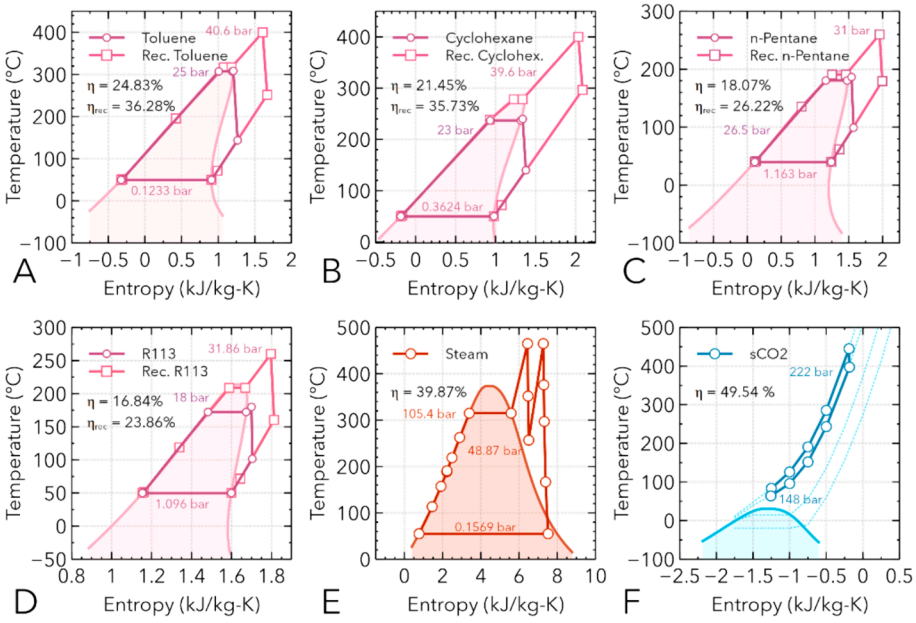

Fig. 9. Temperature-Entropy (T-s) diagrams for the power cycles studied. A: Simple organic and recuperative Rankine cycle with Toluene. B: Simple organic and recuperative Rankine cycle with Cyclohexane. C: Simple and recuperative organic Rankine cycle with n-Pentane. D: Simple organic and recuperative Rankine cycle with R133. E: Reheated Rankine cycle with water vapour. D: Brayton Cycle with supercritical CO_2.

comparable with those of other works with similar conditions analysed, where Schmidt et al. [49] obtained thermal to electrical efficiencies for recuperative ORC close to 41 % and for the steam Rankine cycle of 42 %, from the similar concept of indirect cycles integrated with TCES system based on $Ca(OH)_2/CaO$. In summary, it is shown that the efficiency of the power block in the proposed system will be imposed by the working fluid because the methanation reaction can occur in a wide range of temperatures.

Appendix D summarises the main property values for the state points of each cycle.

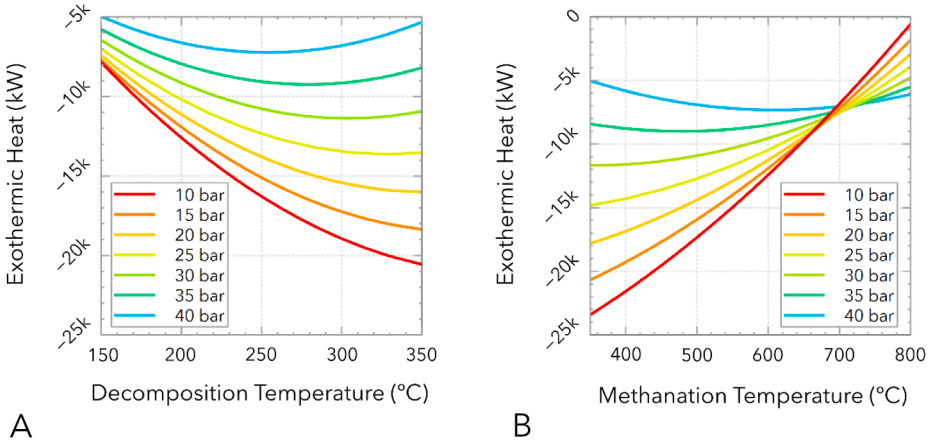

Fig. 10. Variation of the exothermic heat of the discharge phase of the TCES system (methanation reaction) for different methanation pressure levels in each case, as a function of: A. Decomposition temperature of the charging phase, in which the conversion of methanol to syngas is evaluated. B. Methanation temperature in the discharge phase, in which the input of syngas is imposed by the decomposition phase of methanol.

4.1. Sensitivity analysis

One of the most interesting analyses of the above concept resides in the sizing and design of the methanation reactor, which will oversee providing the necessary energy required by the power cycle. In this sense, there is no record of joint analyses of the reaction conditions of thermochemical systems in which the effects of a temperature imposition on the decomposition reactor in the discharge phase are analysed globally. Fig. 10 shows the variation of exothermic heat as a function of the decomposition phase (Fig. 10**A**) and as a function of the discharge phase conditions (Fig. 10**B**). In it, it is observed that the decomposition temperature that makes the conversion maximum in the first instance, with no requirement of recycle currents in the reactor, provides more suitable values for integration with the power block. As the heat expelled by the methanation reaction is higher, the thermal level of the power block will increase, thus providing higher power and a competitive LCOE. This exothermic power in the synthesis phase has a greater influence as the methanation pressure is lower, given the nature of the synthesis reactions. As the temperature in the charge phase is higher (>250 °C), the conversion to syngas will be higher and the by-products of the methane reaction will have a higher mass flow rate and a corresponding higher thermal power. On the other hand, in the discharge phase (Fig. 10**B**), the reaction temperature will be of vital importance, reaching 5 MWt for every 100 °C it increases, according to the values imposed for the installation. Therefore, it is concluded that the methanation pressure is a critical value for the overall evaluation of the system, which cannot be reduced to the minimum possible due to the economic aspects of the installation.

Similarly, one way to evaluate the technical feasibility of the system lies in the analysis of the overall system efficiency (RTE). In this case, a range of temperatures of interest is obtained (Fig. 11), in which the RTE is higher than 50 %, conditioned fundamentally by the conversion of syngas to methane/water from the reaction. Given the nature of the cycles studied, it is obtained that the sCO_2 cycle reaches values of 57 % for the optimal temperature of ~ 450 °C, followed by the steam cycle at ~ 56 % and the recuperative ORC with Toluene at ~ 55.5 %. These values drop sharply as the reaction temperature increases, despite the lower specific CAPEX of the reactor.

Considering the boundary conditions exposed in the previous analyses, the joint evaluation of the discharge reaction pressure and temperature is presented in Fig. 12. Thus, lower methanation pressures are shown to offer better solar-to-electric conversions, that is, better integration efficiency of power blocks. The trend stabilises as temperatures and pressures increase since the kinetics of the reaction stabilises and the energy level at the reactor outlet is higher and usable by the downstream expanders. It follows that as the power cycle power is lower (for ORCs at lower temperatures), the drop in efficiency is of lesser importance because it is the storage system itself that produces energy in its discharge. This means that the system can continue to generate electricity even if the power block undergoes maintenance operations, giving it a certain degree of reliability and response to shut-down operations.

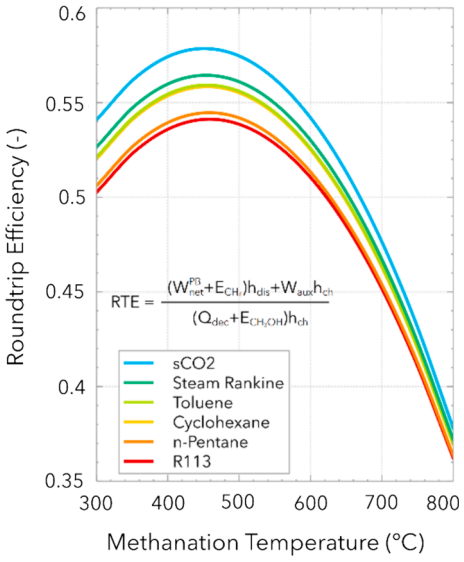

Fig. 11. Effect of variation of the discharge phase methanation temperature on overall system round-trip efficiency. A range of maximum RTE in the temperature range (400–500 °C) is obtained for all the power blocks analysed.

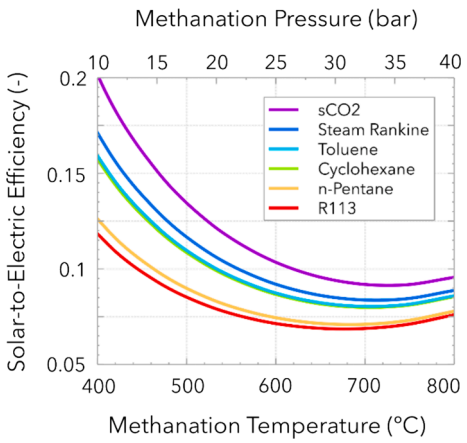

Fig. 12. Effect on solar-to-electric efficiency with a joint variation of methanation reaction temperature and pressure.

4.2. Economic analysis

One of the interesting aspects of the system is its low cost due to its simplicity. This allows for different expansions in its layout, allowing integrations that make it more efficient, which will be studied in later work. In this sense, it is shown that the conditions of the reactions are key to the cost of the whole set because the system is very dependent on the chemical reactions. This is reflected in Fig. 13, which shows the variation in the investment cost of the storage system as a function of the methanation temperature at various pressures. Fundamentally, the cost of the discharge phase will be imposed by the turbomachinery and exchange equipment, with an almost constant cost of the reactor. Therefore, the reactor inlet pressure has a considerable influence on the trends concerning temperatures, as it will be responsible for the sizing of the

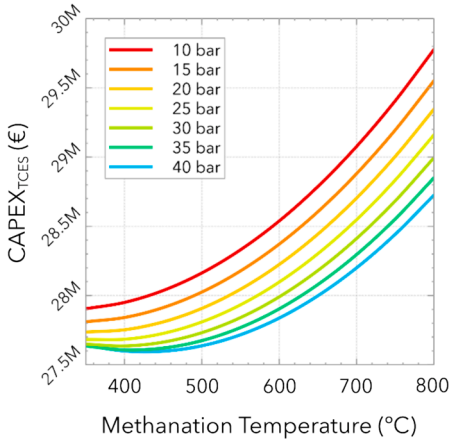

Fig. 13. CAPEX variation of the methanol to methane energy storage system as a function of the methanation temperature, parameterised for different methanation pressures.

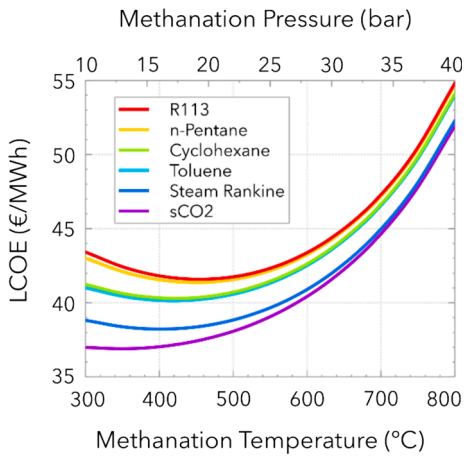

Fig. 14. Variation of the levelized cost of energy (LCOE) as a function of the joint variation of methanation pressure and temperature, studied for recuperative ORC (R113, n-Pentane, Cyclohexane, Toluene), Steam Rankine and Brayton sCO2 power block configurations.

expanders. This CAPEX trend remains minimal and practically linear between 350–500 °C for all pressures, increasing sharply as the reaction temperatures are higher due to higher cost material design and worse thermal integration with the syngas streams at the inlet.

The financial indicator used in this work is the LCOE, which considers the future values of energy flows over the plant's lifetime. This levelized cost is strongly influenced by the energy production in the power block, so the reaction conditions will determine the useful thermal power that can be converted. Therefore, similar trends as in Fig. 13 are expected for the LCOE analysis (Fig. 14). Thus, the working fluids with the lowest thermal to electrical efficiency will be those with the highest levelized energy cost, R113 and n-Pentane, in their recuperative ORC configuration. On the other hand, the most efficient cycles, such as sCO2 and the steam cycle, have increasing cost trends with temperature and pressure, with an approximately constant range between 300–500 °C and 10–20 bar in methanation conditions.

According to the analysis in previous publications in the same field [36], the levelised price of synthetic natural gas production obtained would be less than 180€/MWh, competing with current SNG prices (€165-392/MWh) reported by Götz et al. [66]. These costs depend on the cost of green methanol production, which depends primarily on the cost of green hydrogen for e-methanol and biomass for biomethanol. Estimated production green methanol costs according to IRENA [42] can reduce the levelised fuel cost up to €124/MWh for the biomethanol case and €271/MWh for the e-methanol case, implying that the cost results of this work could be reduced by ~ 1/5 of the assumed assumptions. The LCOEs obtained for the proposed installation are on the order of half of those relative to concentrating solar power plants for power production of € 69–234 / MWh [67] and three times lower than gas turbines burning hydrogen at €1.5/kg, estimated €141-191/MWh by ETN Global [68].

5. Conclusions

This work presents a novel thermochemical energy storage system that employs methanol-to-methane conversion through the intermediate syngas conversion step. In a novel approach in gas-to-gas systems, different power blocks have been integrated with the exothermic methanation reactor, offering competitive RTE values (>55 %), decoupling the reaction conditions with those of the power cycle, making it very flexible. The solar system can offer more than 4000 h of storage in the studied region of southern Europe through a correct design of the storage tanks and the solar field, also demonstrating its scalability. The power cycles studied do not exceed 10 MW of power, and solutions have been proposed for high-temperature fluids that improve the thermal to electrical performances considerably, reaching 50 % in the case of the Brayton case with supercritical CO_2. The improvement in efficiency of the power block allows for economic values comparable to other solar systems, reaching EUR 40/MWh when considering the joint production of natural gas with great high heating value. This configuration offers a possible solution to the massive implementation of renewable fuels in Europe, as it converts renewable methanol (e- /bio-methanol) into synthetic natural gas cleanly and efficiently through CSP, also enabling the integration of a modular power block with existing technology for the simultaneous production of electric power, generating several advantages for stakeholders.

CRediT authorship contribution statement

D.A Rodriguez-Pastor: Writing – original draft, Visualization, Software, Methodology, Investigation, Formal analysis, Data curation, Conceptualization. **I. Marqués-Valderrama:** Writing – review & editing, Methodology. **V.M Soltero:** Writing – review & editing, Validation, Supervision, Conceptualization. **R. Chacartegui:** Writing – review & editing, Validation, Supervision, Methodology, Formal analysis, Conceptualization.

Declaration of competing interest

The authors declare that they have no known competing financial interests or personal relationships that could have appeared to influence the work reported in this paper.

Data availability

Data will be made available on request.

Acknowledgements

ESASUR and VS Energy Tech SL, a spin-off company of the University of Seville, Spain, partially funded this work.

Appendix A:. Kinetic model of MeOH decomposition

Rather than heating steam, the solar energy is used to drive the decomposition of methanol in a solar receiver/reactor to produce syngas. This offers an alternate method of efficiently using solar thermal energy, proposed by Bai et al. [28]. They developed a one-dimensional kinetic model to evaluate a solar methanol thermal decomposition reactor from the *Langmuir-Hinshelwood* rate expression [69]. From their model, validated at pilot scale [70], the kinetic expression of the rate is formulated in **Eq. (A1)**:

$$r_D = \frac{k_D K^*_{CH_3O^{(2)}} \left(\frac{p_{CH_3OH}}{p^{0.5}_{H_2}}\right)\left(1 - \frac{p^2_{H_2} p_{CO}}{k_D p_{CH_3OH}}\right) C^T_{S_2} C^T_{S_{2a}}}{\left[1 + K^*_{CH_3O^{(2)}}\left(\frac{p_{CH_3OH}}{p^{0.5}_{H_2}}\right)\right]\left(1 + K_{H^{(2a)}} p^{0.5}_{H_2}\right)} \tag{A1}$$

where C is the total surface of concentration, p the partial pressure of each species, k the rate constant of the reaction and K the equilibrium constant of the decomposition reaction. From the *Arrhenius* equation or the *Van't Hoff* equation, the equilibrium constant and rate can be expressed as a function of temperature, as shown in **Eqs. (A2), (A3)** and **(A4)**.

$$k_D = k^{\infty}_D \exp\left(-\frac{E_D}{RT}\right) \tag{A2}$$

$$K^*_{CH_3O^{(2)}} = \exp\left(\frac{\Delta S^*_{CH_3O^{(2)}}}{R} - \frac{\Delta H^*_{CH_3O^{(2)}}}{RT}\right) \tag{A3}$$

$$K_{H^{(2a)}} = \exp\left(\frac{\Delta S^*_{H^{(2a)}}}{R} - \frac{\Delta H^*_{H^{(2a)}}}{RT}\right) \tag{A4}$$

R being the universal gas constant (8.314 J/mol-K), ΔH^*_i the enthalpy of formation of the corresponding species, S the entropy, E the activation energy and T the reaction temperature. Reference values for the kinetic constants are listed in Table A1:

Table A1
Values for the kinetic model of the thermal decomposition of methanol with Cu/ZnO/Al_2O_3 porous catalyst.

Constant	ΔS^*_i (J/mol-K) or k^{∞}_i (m^2/s-mol)	ΔH^*_i (kJ/mol) or E(kJ/mol)
$K^*_{CH_3O^{(2)}}$	30.0	−20.0
$K_{H^{(2a)}}$	−46.2	−50.0
k^{∞}_D	3.8×10^{20}	170

Reference values for the catalytic simulation in ASPEN HYSYS are shown in Table A2:

Table A2
Values for Cu/ZnO/Al_2O_3 porous catalyst and catalyst bed properties.

Property	Value
Catalyst particle composition	40 wt% CuO, 40 wt% ZnO, 20 wt% Al_2O_3
Catalyst density	5676 kg/m^3
Catalyst bed porosity	0.49
Specific surface area	102 m^2/g

Appendix B:. Kinetic model of syngas methanation

Burger et al. [71] focused on the kinetic description of the above reaction system catalysed by a co-precipitated, hydrotalcite-derived $NiAlO_x$ catalyst. For commercial Ni/Al_2O_3 catalysts (50 wt% Ni/Al_2O_3, Specific surface area = 183 m^2/g), Kopyscinski [72] developed a kinetic model of CO methanation in which the rate equations were adapted by Er-rbib et al. [62] for multistage adiabatic reactors (**Eqs. (B1), (B2), (B3)**):

$$r_{meth} = \frac{k_1 \cdot 10^{-3} K_1 p^{0.5}_{CO} p^{0.5}_{H_2}}{\left(1 + K_1 p^{0.5}_{CO} + K_2 p_{H_2O} p^{-0.5}_{H_2}\right)^2} (\text{kmol/kg·s}) \tag{B1}$$

$$r_{WGS} = \frac{k_2 \cdot 10^{-3}\left(K_3 p_{CO} p_{H_2O} p^{-0.5}_{H_2} - K_4 p_{CO_2} p^{0.5}_{H_2}\right)}{\left(1 + K_1 p^{0.5}_{CO} + K_2 p_{H_2O} p^{-0.5}_{H_2}\right)^2} (\text{kmol/kg·s}) \tag{B2}$$

$$\ln K_i = A_i + B_i/T \tag{B3}$$

This kinetic model was validated based on data from simulations and industrial plants [73], where the values of the parameters that adjust the kinetics of the reaction are listed in Table B1.

Table B1
Fitting parameters for the kinetic reaction of methanation for multistage adiabatic reactors [62].

Equilibrium constant	Parameter	Value
K_1	A_1	–23.24
	B_1	7355.77
K_2	A_2	−20.49
	B_2	8731.97
K_3	A_3	−19.64

(*continued on next page*)

Table B1 (*continued*)

Equilibrium constant	Parameter	Value
	B_3	781.25
K_4	A_4	−13.208
	B_4	−4400

Appendix C:. Economic approach

Table C1
Cost-correlation mathematical expressions for the proposed methanol-to-methane TCES system.

Equipment	Scaling parameter	Expression	Ref.
Endothermic reactor	Thermal power (kW)	$IC_{Dr} = 13140 \bullet \dot{Q}_r^{0.67}$	[74]
Exothermic Reactor	Thermal power (kW)	$IC_{Mr} = 19594 \bullet \dot{Q}_r^{0.5}$	[74]
Compressors	Power (kW)	$IC_C = 643.15 \bullet \dot{W}_C^{0.9142}$	[75]
Expanders	Power (kW)	$IC_{exp} = 4001.4 \bullet \dot{W}_{exp}^{0.6897}$	[76]
Pump	Power (kW) and pump efficiency (−)	$IC_P = 3531.4 \bullet \dot{W}_P^{0.71} \bullet \left[1+\left(\frac{1-0.8}{1-\eta_{i,P}}\right)^3\right]$	[77]
Heat Exchangers	Area (m^2) and pressure (bar)	$IC_{HE} = 2546.9 \bullet A_{HE}^{0.67} \bullet P_{HE}^{0.28} \bullet 10^{-6}$	[77]
Cooler	Cooling power (kW)	$IC_{Cooling}^{tower} = 32.3 \bullet \dot{Q}_{cool}$	[78]
Tanks	Volume (m^3)	$IC_{Tank} = 83 \cdot V_{tank}$	[79]
Solar Photovoltaic Field	Power (kW)	$IC_{PV} = 0.995 \cdot \dot{W}_{PV} \cdot 10^3$	[80]
CSP field (PTC-based)	Receiver thermal power (kW)	$IC_{rec}^{solar} = 57.07 \bullet \Phi_{Receiver}$	[81]

Table C2
Cost reference values according to the CEPCI index of the power block were integrated with the TCES system [59].

Power Block	Equipment	C_{ref}(kEUR)	S_{ref}	m(−)
Organic Rankine Cycle	Pump	7.5	1000 kW	0.58
	Expander	25	1000 kW	0.68
	Generator	3.7	10.000 kW	0.95
	Cooling Tower	72	3600 kW	1
	Heat exchangers	21	100 m^2	0.71
Steam Rankine Cycle	Pump	7.5	1000 kW	0.58
	Turbine	25	1000 kW	0.68
	Generator	3.7	10.000 kW	0.95
	Cooling Tower	72	3600 kW	1
	Heat exchangers	21	100 m^2	0.71
sCO2 Brayton Cycle	Gas turbine	6800	$4 \cdot 10^6$ kW	0.53
	Generator	3.7	10.000 kW	0.95
	Cooling Tower	72	3600 kW	1
	Heat exchangers	21	100 m^2	0.71

Appendix D:. State points

Table D1
Methanol to syngas charge phase state points.

Stream	Temperature (°C)	Pressure (bar)	CO Molar fraction (−)	H_2 Molar fraction (−)	CH_3OH Molar fraction (−)	Molar Flow (kmol/h)	Molar Enthalpy (kJ/kmol)	Molar Entropy (kJ/kmol-K)
1	25.00	0.14	0.00	0.00	1.00	360.00	−241884.84	16.44
2	25.17	10.00	0.00	0.00	1.00	360.00	−241831.26	16.44
3	25.17	10.00	0.00	0.00	1.00	360.00	−241831.26	16.44
4	134.11	10.00	0.00	0.00	1.00	360.00	−228520.88	54.28
5	139.20	10.00	0.00	0.00	1.00	360.00	−214396.34	88.54
6	315.00	10.00	0.333	0.667	0.00	1074.96	−28796.54	141.16
7	154.11	10.00	0.333	0.667	0.00	1074.96	−33526.78	131.77
8	30.00	10.00	0.00	0.00	1.00	2.52	−241288.24	18.25
9	30.00	10.00	0.333	0.667	0.00	1074.96	−35967.64	125.41
10	197.72	40.00	0.333	0.667	0.00	1072.44	−31871.14	122.86
11	45.17	40.00	0.333	0.667	0.00	1072.44	−36339.19	111.39

Table D2
Syngas to methane discharge phase state points.

Stream	Temperature (°C)	Pressure (bar)	CO Molar fraction (—)	H_2 Molar fraction (—)	CH_4 Molar fraction (—)	H_2O Molar fraction (—)	Molar Flow (kmol/h)	Molar Enthalpy (kJ/kmol)	Molar Entropy (kJ/kmol-K)
12	45.17	40.00	0.333	0.667	0.00	0.00	1072.44	−36339.19	111.39
13	127.51	40.00	0.333	0.667	0.00	0.00	1072.44	−33929.37	118.13
14	98.07	30.00	0.333	0.667	0.00	0.00	1072.44	−34785.00	118.33
15	160.64	30.00	0.333	0.667	0.00	0.00	1072.44	−32958.93	122.87
16	450.00	30.00	0.202	0.009	0.3942	0.3942	706.43	−81428.59	189.82
17	277.44	1.00	0.202	0.009	0.3942	0.3942	706.43	−100801.55	193.02
18	277.44	1.00	0.202	0.009	0.3942	0.3942	353.22	−100801.55	193.02
19	277.44	1.00	0.202	0.009	0.3942	0.3942	353.22	−100801.55	193.02
20	118.07	1.00	0.202	0.009	0.3942	0.3942	353.22	−106345.93	181.16
21	65.67	1.00	0.202	0.009	0.3942	0.3942	353.22	−108118.31	176.29
22	91.28	1.00	0.202	0.009	0.3942	0.3942	706.43	−107232.65	178.81
23	25.00	1.00	0.3229	0.0155	0.6303	0.00	540.36	−68659.04	166.84
24	25.00	1.00	0.00	0.00	0.00	1.00	706.43	−119806.16	140.24

Table D3
ORC cycle state points integrated with TCES system for various working fluids.

State	Toluene		Cyclohexane		n-Pentane		R113	
	Temperature (°C)	Pressure (bar)	Temperature (°C)	Pressure (bar)	Temperature (°C)	Pressure (bar)	Temperature (°C)	Pressure (bar)
1	51.65	40.6	51.75	39.6	41.59	31	55.08	31.86
2	195.7	40.6	237.4	39.6	135.6	31	120.3	31.86
3	400	40.6	400	39.6	260	31	260	31.86
4	251.7	0.1233	295.6	0.3624	179.6	1.163	162.9	1.096
5	71.65	0.1233	71.75	0.3624	61.59	1.163	75.08	1.096
6	30	0.1233	30	0.3624	20	1.163	30	1.096
Mass Flow Rate (kg/s)	16.78		17.64		21.1		53.08	

Table D4
Steam Rankine cycle state points integrated with TCES system.

State	Temperature (°C)	Pressure (bar)	Flow Rate (kg/s)
1	54.91	0.1569	3.603
3	113.4	12.17	3.603
4	157.2	12.17	3.603
5	188.6	12.17	4.482
7	218.8	105.3	4.482
8	262.6	105.3	4.482
9	465	105.3	4.482
10	351.9	48.87	0.4717
12	257	22.66	0.2344
13	465	22.66	3.776
14	376.1	12.17	0.1736
15	297.3	6.537	0.2827
16	166.8	1.886	0.3572
17	54.91	0.1569	3.603

Table D5
Supercritical CO2 cycle state points integrated with TCES system.

State	Temperature (°C)	Pressure (bar)
1	31.84	148
2	15	148
3	20.84	222
4	375.1	222
5	439	222
6	391.5	148
Mass Flow Rate (kg/s)	143.8	

References

[1] Chu S, Cui Y, Liu N. The path towards sustainable energy. Nat Mater 2017;16:16–22. https://doi.org/10.1038/nmat4834.

[2] Commission on the Geopolitics of Energy Transformation G. A new world: The geopolitics of the energy transformation 2019.

[3] Ben Cheikh N, Ben ZY. Renewable energy deployment and geopolitical conflicts. J Environ Manage 2023:344. https://doi.org/10.1016/J.JENVMAN.2023.118561.

[4] Ah-Voun D, Chyong CK, Li C. Europe's energy security: from Russian dependence to renewable reliance. Energy Policy 2024;184:113856. https://doi.org/10.1016/j.enpol.2023.113856.

[5] Falkner R. The Paris Agreement and the new logic of international climate politics. Int Aff 2016;92:1107–25. https://doi.org/10.1111/1468-2346.12708.

[6] Ipakchi A, Albuyeh F. Grid of the future. IEEE Power Energ Mag 2009;7:52–62. https://doi.org/10.1109/MPE.2008.931384.

[7] Arteconi A, Hewitt NJ, Polonara F. State of the art of thermal storage for demand-side management. Appl Energy 2012;93:371–89. https://doi.org/10.1016/J.APENERGY.2011.12.045.

[8] Pelay U, Luo L, Fan Y, Stitou D, Rood M. Thermal energy storage systems for concentrated solar power plants. Renew Sustain Energy Rev 2017;79:82–100. https://doi.org/10.1016/J.RSER.2017.03.139.

[9] Cole W, Frazier AW, Augustine C. Cost Projections for Utility-Scale Battery Storage: 2021 Update 2021. 10.2172/1786976.

[10] Prestigiacomo C, Proietto F, Giaconia A, Genovesi M, Hamdi N, Scialdone O, et al. Solar heat for the decarbonization of chemical industry: dehydrogenation of ethylbenzene to styrene driven by a concentrating solar power plant with molten salts as heat transfer fluids. Energy Conversion and Management: X 2024;22:100546. https://doi.org/10.1016/J.ECMX.2024.100546.

[11] Xu B, Li P, Chan C. Application of phase change materials for thermal energy storage in concentrated solar thermal power plants: a review to recent developments. Appl Energy 2015;160:286–307. https://doi.org/10.1016/j.apenergy.2015.09.016.

[12] Chen X, Zhang Z, Qi C, Ling X, Peng H. State of the art on the high-temperature thermochemical energy storage systems. Energy Convers Manag 2018;177:792–815. https://doi.org/10.1016/J.ENCONMAN.2018.10.011.

[13] Zhang D, Yang X, Li H, Jia Z, Zhang S, Tang S, et al. 4E analysis and parameter study of a solar-thermochemical energy storage CCHP system. Energy Convers Manag 2024;301:118002. https://doi.org/10.1016/J.ENCONMAN.2023.118002.

[14] Zhang N, Wang Z, Lior N, Han W. Advancement of distributed energy methods by a novel high efficiency solar-assisted combined cooling, heating and power system. Appl Energy 2018;219:179–86. https://doi.org/10.1016/j.apenergy.2018.03.050.

[15] Bai Z, Liu Q, Lei J, Li H, Jin H. A polygeneration system for the methanol production and the power generation with the solar-biomass thermal gasification. Energy Convers Manag 2015;102:190–201. https://doi.org/10.1016/j.enconman.2015.02.031.

[16] Rodríguez-Pastor DA, Carvajal E, Becerra JA, Soltero VM, Chacartegui R. Methanol-based thermochemical energy storage (TCES) for district heating networks. Energy 2024;298:131292. https://doi.org/10.1016/J.ENERGY.2024.131292.

[17] Carro A, Chacartegui R, Ortiz C, Becerra JA. Indirect power cycles integration in concentrated solar power plants with thermochemical energy storage based on calcium hydroxide technology. J Clean Prod 2023;421:138417. https://doi.org/10.1016/J.JCLEPRO.2023.138417.

[18] Carro A, Chacartegui R, Ortiz C, Arcenegui-Troya J, Pérez-Maqueda LA, Becerra JA. Integration of calcium looping and calcium hydroxide thermochemical systems for energy storage and power production in concentrating solar power plants. Energy 2023;283:128388. https://doi.org/10.1016/J.ENERGY.2023.128388.

[19] André L, Abanades S. Evaluation and performances comparison of calcium, strontium and barium carbonates during calcination/carbonation reactions for solar thermochemical energy storage. J Energy Storage 2017;13:193–205. https://doi.org/10.1016/J.EST.2017.07.014.

[20] Dunn R, Lovegrove K, Burgess G. A review of ammonia-based thermochemical energy storage for concentrating solar power. Proc IEEE 2012;100:391–400. https://doi.org/10.1109/JPROC.2011.2166529.

[21] Rodriguez-Pastor DA, Carro A, Masci G, Ortiz C, Verda V, Chacartegui R. Conceptualizing novel CH3OH-based thermochemical energy storage routes via a modeling approach. Cell Rep Phys Sci 2023:101357. https://doi.org/10.1016/J.XCRP.2023.101357.

[22] Janz GJ, Allen CB, Bansal NP, Murphy RM, Tomkins RPT, Janz GJ, et al. Physical properties data compilations relevant to energy storage, 2. molten salts: data on single and multi-component salt systems. STIN 1979;80:10643.

[23] Ortiz C, Chacartegui R, Valverde JM, Alovisio A, Becerra JA. Power cycles integration in concentrated solar power plants with energy storage based on calcium looping. Energy Convers Manage 2017. https://doi.org/10.1016/j.enconman.2017.03.029.

[24] Tesio U, Guelpa E, Verda V. Integration of thermochemical energy storage in concentrated solar power. Part 2: comprehensive optimization of supercritical CO2 power block. Energy Conversion and Management: X 2020;6:100038. https://doi.org/10.1016/J.ECMX.2020.100038.

[25] Peng X, Yao M, Root TW, Maravelias CT. Design and analysis of concentrating solar power plants with fixed-bed reactors for thermochemical energy storage. Appl Energy 2020;262:114543. https://doi.org/10.1016/J.APENERGY.2020.114543.

[26] Dunn R, Lovegrove K, Burgess G. A review of ammonia-based thermochemical energy storage for concentrating solar power. Proc IEEE 2012;100:391–400. https://doi.org/10.1109/JPROC.2011.2166529.

[27] Chen C, Aryafar H, Warrier G, Lovegrove KM, Lavine AS. Ammonia synthesis for producing supercritical steam in the context of solar thermochemical energy storage. AIP Conf Proc 2016:1734. https://doi.org/10.1063/1.4949108/997084.

[28] Bai Z, Liu Q, Lei J, Jin H. Investigation on the mid-temperature solar thermochemical power generation system with methanol decomposition. Appl Energy 2018;217:56–65. https://doi.org/10.1016/J.APENERGY.2018.02.101.

[29] Bristowe G, Smallbone A. The key techno-economic and manufacturing drivers for reducing the cost of power-to-gas and a hydrogen-enabled energy system. Hydrogen. 2021;2:273–300. https://doi.org/10.3390/HYDROGEN2030015.

[30] Mazloomi K, Gomes C. Hydrogen as an energy carrier: prospects and challenges. Renew Sustain Energy Rev 2012;16:3024–33. https://doi.org/10.1016/J.RSER.2012.02.028.

[31] Lan R, Tao S. Ammonia as a suitable fuel for fuel cells. Front Energy Res 2014;2:110206. https://doi.org/10.3389/FENRG.2014.00035/BIBTEX.

[32] CRC Handbook of Chemistry and Physics. CRC Handbook of Chemistry and Physics 2016. 10.1201/9781315380476.

[33] Müller K, Fabisch F, Arlt W. Energy transport and storage using methanol as a carrier. Green 2014;4:19–25. https://doi.org/10.1515/GREEN-2013-0028/MACHINEREADABLECITATION/RIS.

[34] Schorn F, Breuer JL, Samsun RC, Schnorbus T, Heuser B, Peters R, et al. Methanol as a renewable energy carrier: an assessment of production and transportation costs for selected global locations. Adv Appl Energy 2021;3:100050. https://doi.org/10.1016/J.ADAPEN.2021.100050.

[35] CHACARTEGUI RAMÍREZ R, BECERRA VILLANUEVA JA, VALVERDE MILLÁN JM, ORTIZ DOMÍNGUEZ C, MASCI G. (2019) ES2792748B2 - Instalacion de almacenamiento de energia termoquimicamecanica y procedimiento de almacenamiento de energia.

[36] Rodriguez-Pastor DA, Garcia-Guzman A, Marqués-Valderrama I, Ortiz C, Carvajal E, Becerra JA, et al. A flexible methanol-to-methane thermochemical energy storage system (TCES) for gas turbine (GT) power production. Appl Energy 2024;356:122398. https://doi.org/10.1016/J.APENERGY.2023.122398.

[37] Chacartegui R, Sánchez D, Muñoz de Escalona JM, Muñoz A, Sánchez T. Gas and steam combined cycles for low calorific syngas fuels utilisation. Appl Energy 2013;101:81–92. https://doi.org/10.1016/J.APENERGY.2012.02.041.

[38] From solid fuels to substitute natural gas (SNG) using TREMP^{TM} Topsøe Recycle Energy-efficient Methanation Process n.d.

[39] Schrems I, Wieland P, Schenuit C, Fiedler S. Pricing methane Implementing a methane pricing model for the EU gas market On behalf of 2021.

[40] Marks L. (2022) The Abatement Cost of Methane Emissions from Natural Gas Production. Https://DoiOrg/101086/716700 2022;9:165–98. 10.1086/716700.

[41] Hausman C, Muehlenbachs L. Price regulation and environmental externalities: evidence from methane leaks. J Assoc Environ Resour Econ 2019;6:73–109. https://doi.org/10.1086/700301/ASSET/IMAGES/LARGE/FG2.JPEG.

[42] IRENA AND METHANOL INSTITUTE. Innovation Outlook : Renewable Methanol. Abu Dhabi: 2021.

[43] Islam MT, Huda N, Abdullah AB, Saidur R. A comprehensive review of state-of-the-art concentrating solar power (CSP) technologies: current status and research trends. Renew Sustain Energy Rev 2018;91:987–1018. https://doi.org/10.1016/j.rser.2018.04.097.

[44] Chen X, Zhang Z, Qi C, Ling X, Peng H. State of the art on the high-temperature thermochemical energy storage systems. EnergyConvers Manag 2018;177:792–815. https://doi.org/10.1016/J.ENCONMAN.2018.10.011.

[45] Wong B, Brown L, Buckingham R, Sweet W, Russ B, Gorensek M. Sulfur dioxide disproportionation for sulfur based thermochemical energy storage. Sol Energy 2015;118:134–44. https://doi.org/10.1016/J.SOLENER.2015.04.037.

[46] Peng X, Root TW, Maravelias CT. Storing solar energy with chemistry: the role of thermochemical storage in concentrating solar power. Green Chem 2017;19:2427–38. https://doi.org/10.1039/C7GC00023E.

[47] Formica M, Frigo S, Gabbrielli R. Development of a new steady state zero-dimensional simulation model for woody biomass gasification in a full scale plant. Energy Convers Manag 2016;120:358–69. https://doi.org/10.1016/J.ENCONMAN.2016.05.009.

[48] Lai NA, Wendland M, Fischer J. Working fluids for high-temperature organic Rankine cycles. Energy 2011;36:199–211. https://doi.org/10.1016/J.ENERGY.2010.10.051.

[49] Schmidt M, Linder M. Power generation based on the Ca(OH)2/ CaO thermochemical storage system – experimental investigation of discharge operation modes in lab scale and corresponding conceptual process design. Appl Energy 2017;203:594–607. https://doi.org/10.1016/j.apenergy.2017.06.063.

[50] Quoilin S, Van Den BM, Declaye S, Dewallef P, Lemort V. Techno-economic survey of Organic Rankine Cycle (ORC) systems. Renew Sustain Energy Rev 2013;22:168–86. https://doi.org/10.1016/J.RSER.2013.01.028.

[51] Turchi CS, Ma Z, Neises TW, Wagner MJ. Thermodynamic study of advanced supercritical carbon dioxide power cycles for concentrating solar power systems. J Solar Energy Eng, Transactions of the ASME. 2013;135. https://doi.org/10.1115/1.4024030/368503.

[52] Ortiz C, Chacartegui R, Valverde JM, Alovisio A, Becerra JA. Power cycles integration in concentrated solar power plants with energy storage based on calcium looping. Energy Convers Manag 2017;149:815–29. https://doi.org/10.1016/J.ENCONMAN.2017.03.029.

[53] Carro A, Chacartegui R, Ortiz C, Carneiro J, Becerra JA. Energy storage system based on transcritical CO2 cycles and geological storage. Appl Therm Eng 2021;193:116813. https://doi.org/10.1016/J.APPLTHERMALENG.2021.116813.

[54] Hou Z, Zheng D, Jin H, Sui J. Performance analysis of non-isothermal solar reactors for methanol decomposition. Sol Energy 2007;81:415–23. https://doi.org/10.1016/J.SOLENER.2006.04.007.

[55] Moreno A, Gilabert MA, Martínez B. Mapping daily global solar irradiation over Spain: a comparative study of selected approaches. Sol Energy 2011;85:2072–84. https://doi.org/10.1016/J.SOLENER.2011.05.017.
[56] Rodriguez-Pastor DA, Ildefonso-Sanchez AF, Soltero VM, Peralta ME, Chacartegui R. A new predictive model for the design and evaluation of bifacial photovoltaic plants under the influence of vegetation soils. J Clean Prod 2023;385:135701. https://doi.org/10.1016/J.JCLEPRO.2022.135701.
[57] PVsyst. PVsyst – Logiciel Photovoltaïque 2022. https://www.pvsyst.com/ (accessed September 9, 2022).
[58] Hussain I, Jalil AA, Hassan NS, Hamid MYS. Recent advances in catalytic systems for CO2 conversion to substitute natural gas (SNG): perspective and challenges. J Energy Chem 2021;62:377–407. https://doi.org/10.1016/J.JECHEM.2021.03.040.
[59] Jenkins S. Construction-cost indices. Chem Eng 2014;121:28–9.
[60] IEA. Renewable Methanol. 2021.
[61] Hou Z, Zheng D, Jin H, Sui. Performance analysis of non-isothermal solar reactors for methanol decomposition. Sol Energy 2007;81:415–23. https://doi.org/10.1016/J.SOLENER.2006.04.007.
[62] Er-rbib H, Bouallou C. Modeling and simulation of CO methanation process for renewable electricity storage. Energy 2014;75:81–8. https://doi.org/10.1016/J.ENERGY.2014.05.115.
[63] Lazard. 2023 Levelized Cost Of Energy+ | Lazard 2023. https://www.lazard.com/research-insights/2023-levelized-cost-of-energyplus/ (accessed April 29, 2023).
[64] Escamilla A, Sánchez D, García-Rodríguez L. Techno-economic study of power-to-power renewable energy storage based on the smart integration of battery, hydrogen, and micro gas turbine technologies. Energy Conversion and Management: X 2023;18:100368. https://doi.org/10.1016/J.ECMX.2023.100368.
[65] Steilen M, Jörissen L. Hydrogen conversion into electricity and thermal energy by fuel cells: use of H2-systems and batteries. Electrochemical Energy Storage for Renewable Sources and Grid Balancing 2015:143–58. https://doi.org/10.1016/B978-0-444-62616-5.00010-3.
[66] Götz M, Lefebvre J, Mörs F, McDaniel Koch A, Graf F, Bajohr S, et al. Renewable Power-to-Gas: a technological and economic review. Renew Energy 2016;85:1371–90. https://doi.org/10.1016/J.RENENE.2015.07.066.
[67] Badouard T, Moreira De Oliveira D, Yearwood J, Torres P. (2020) Final Report-Cost of Energy (LCOE) Study on energy costs, taxes and the impact of government interventions on investments in the energy sector.
[68] ETN Global. (2022) HYDROGEN DEPLOYMENT IN CENTRALISED POWER GENERATION A techno-economic case study HYDROGEN DEPLOYMENT IN CENTRALISED POWER GENERATION-A TECHNO-ECONOMIC CASE STUDY.
[69] Lee JK, Ko JB, Kim DH. Methanol steam reforming over Cu/ZnO/Al2O3 catalyst: kinetics and effectiveness factor. Appl Catal A Gen 2004;278:25–35. https://doi.org/10.1016/J.APCATA.2004.09.022.
[70] Liu T, Liu Q, Xu D, Sui J. Performance investigation of a new distributed energy system integrated a solar thermochemical process with chemical recuperation. Appl Therm Eng 2017;119:387–95. https://doi.org/10.1016/j.applthermaleng.2017.03.073.
[71] Burger T, Donaubauer P, Hinrichsen O. On the kinetics of the co-methanation of CO and CO2 on a co-precipitated Ni-Al catalyst. Appl Catal B 2021;282:119408. https://doi.org/10.1016/J.APCATB.2020.119408.
[72] Kopyscinski J. Production of synthetic natural gas in a fluidized bed reactor: understanding the hydrodynamic, mass transfer and kinetic effects. Disseration ETH Zurich 2010.
[73] Davis C, Arcilla N, Hui M, Hutchins B. (1981) Methanation plant design for HTGR process heat. 10.2172/6104352.
[74] Michalski S, Hanak DP, Manovic V. Techno-economic feasibility assessment of calcium looping combustion using commercial technology appraisal tools. J Clean Prod 2019;219:540–51. https://doi.org/10.1016/J.JCLEPRO.2019.02.049.
[75] Carlson M, … BM-E, (2017) undefined. Techno-economic comparison of solar-driven SCO2 Brayton cycles using component cost models baselined with vendor data and estimates. AsmedigitalcollectionAsmeOrg n.d.
[76] Carlson M, Middleton B, Ho C. Techno-economic comparison of solar-driven SCO2 Brayton cycles using component cost models baselined with vendor data and estimates. Energy Sustainability 2017. https://doi.org/10.1115/ES2017-3590 (V001T05A009).
[77] Michalski S, Hanak D, Production VM-J of C, (2019) undefined. Techno-economic feasibility assessment of calcium looping combustion using commercial technology appraisal tools. Elsevier n.d.
[78] Michalski S, Hanak DP, Manovic V. Techno-economic feasibility assessment of calcium looping combustion using commercial technology appraisal tools. J Clean Prod 2019;219:540–51. https://doi.org/10.1016/J.JCLEPRO.2019.02.049.
[79] Bayon A, Bader R, Jafarian M, Energy LF-H-. (2018) undefined. Techno-economic assessment of solid–gas thermochemical energy storage systems for solar thermal power applications. Elsevier n.d.
[80] - International Energy Agency I. Renewables 2022 2022.
[81] Ho CK. A review of high-temperature particle receivers for concentrating solar power. Appl Therm Eng 2016;109:958–69. https://doi.org/10.1016/J.APPLTHERMALENG.2016.04.103.